Diffraction study of calcium aluminate glasses and melts: II. High energy x-ray diffraction on melts

2008 J. Phys.: Condens. Matter 20 245107

(http://iopscience.iop.org/0953-8984/20/24/245107)

J. Phys.: Condens. Matter **20** (2008) 245107 (7pp) doi:10.1088/0953-8984/20/24/245107

Diffraction study of calcium aluminate glasses and melts: II. High energy x-ray diffraction on melts

Q Mei[1,5], C J Benmore[1,2], J K R Weber[3,6], M Wilding[4], J Kim[3,7] and J Rix[3,6]

[1] Intense Pulsed Neutron Source, Argonne National Laboratory, IL 60439, USA
[2] X-ray Science Division, Advanced Photon Source, Argonne National Laboratory, IL 60439, USA
[3] Containerless Research Inc., Evanston, IL 60202, USA
[4] Institute of Mathematical and Physical Sciences, University of Wales, Aberystwyth, Cerdigion SY23 3BZ, UK

Received 14 January 2008, in final form 7 May 2008
Published 29 May 2008
Online at stacks.iop.org/JPhysCM/20/245107

Abstract

High energy x-ray diffraction measurements have been performed on $CaO–Al_2O_3$ liquids suspended in a flow of pure argon for six compositions containing 50–67 mol% CaO. The results indicate that AlO_4 tetrahedra dominate the liquid structure. The radial distribution functions show a significant broadening of the Ca–O peak occurs in the liquid compared to the corresponding glass and, on average, each Ca is surrounded by approximately five oxygen atoms in the melt at a distance of 2.3 Å. It is also found that the structure for the eutectic (64% CaO) liquid does not change measurably with temperature between 1600 and 1970 °C.

(Some figures in this article are in colour only in the electronic version)

1. Introduction

The distorted Ca–O environment in calcium aluminate (CA) glasses described in our preceding paper [1] has stimulated a study of the liquid structure using combined levitation and high energy x-ray diffraction. In CA glasses around the eutectic the oxygen coordination around Ca has been found to be four at a well-defined distance of 2.4 Å, more commonly associated with an octahedral arrangement, with an additional smaller coordination covering a broader range at longer distances. The role of the Ca ion in these liquids may be linked to the findings of McMillan and coworkers, who have suggested that changes in the CA Raman spectra above T_g may be associated with the formation of highly coordinated Al species in the melt or a modification in the polymerization state of the aluminate network [2–5]. However, these authors have pointed out that this is difficult to reconcile with the main changes in Raman intensity and suggested that x-ray diffraction or IR spectroscopy be used to identify the structural changes. Large configurational changes shown in the Raman spectra of CA glasses above T_g have been interpreted with the formation of OAl_3 triclusters, i.e. three tetrahedral Al atoms each sharing the same oxygen [4]. In this model O^{2-} ions are removed from the fully polymerized aluminate framework to become coordinated by Ca^{2+} ions, although it has been noted that these changes appear to be rapidly reversible upon quenching the melt [5].

Liquid 50% CaO:50% Al_2O_3 exhibits a highly non-Arrhenius behavior in the melt, forming an extremely fragile liquid [2, 6]. Poe *et al* [2, 3] performed ^{27}Al NMR measurements and ion dynamics simulations on liquid CA binaries containing 30–70 mol% CaO and the results indicated that the Al coordination at the 50% CaO composition is close to four, although some small quantities of five-and sixfold coordinate Al are also present. Their ion dynamics simulations [2, 3] also showed that the average coordination of Al by oxygen in the liquids increases from 4.2 at the eutectic (64 mol% CaO) composition to 4.5 at the equimolar (50 mol% CaO) composition, with the proportion of five-and sixfold Al species increasing as the temperature is increased. The relevant part of the CA phase diagram is shown in figure 1.

[5] Present address: HP-CAT, Advanced Photon Source, Argonne National Laboratory, IL 60439, USA.
[6] Present address: Materials Development, Inc., Arlington Heights, IL 60004, USA.
[7] Present address: Department of Materials Science and Engineering, Northwestern University, Evanston, IL 60208, USA.

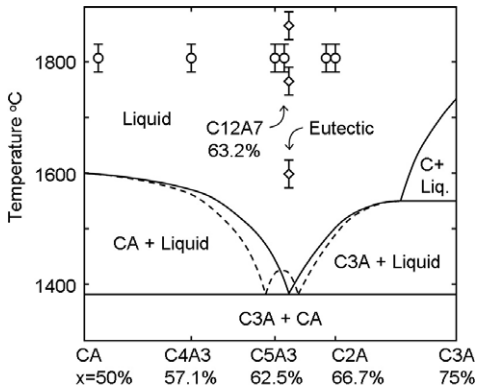

Figure 1. Sketch of the $(CaO)x\cdot(Al_2O_3)(1-x)$ phase diagram around the eutectic composition based on reports by Chatterjee *et al* [27] (dashed line) and Nurse *et al* [28] (solid line), where C represents CaO and A represents Al_2O_3. The compositions and temperatures of the liquids used in this experiment are shown as circles, except for the eutectic composition which are shown as diamonds.

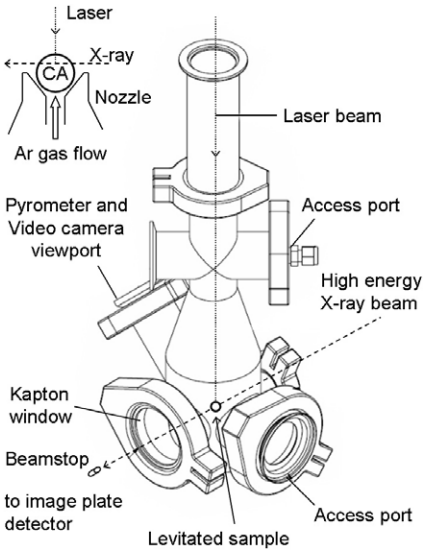

Figure 2. The conical nozzle levitator enclosure on beamline 11-ID-C at the APS showing a class 1 system which contains the embedded class 4 laser. The high energy x-ray and laser beams are coincident on the top half of the levitated CA bead (cross section view in top left corner) and the apparent temperature is monitored through an oblique 45° view port. The x-ray beam exit angle is nominally 20° to allow a maximum Q value of ~20 $Å^{-1}$ to be obtained using an incident energy of 115 keV.

In this work we have studied the structure of CA liquids for six compositions containing from 50 to 67 mol% CaO (either side of the eutectic) using a combination of high energy x-ray diffraction, an aerodynamic levitation system and a large-area image plate detector.

2. Experimental details

The sample environment of the CA melts was controlled using aerodynamic levitation with a 240 W continuous-wave CO_2 laser beam heating system. Similar techniques have been applied in prior work [7] but in this study we have integrated the system on a high energy x-ray diffraction beamline [8]. The advantages of high energy diffraction for bulk liquid and glass studies include small attenuation and multiple scattering effects on millimeter-sized samples and the ability to access large momentum transfers [9]. The levitator was enclosed in a purpose-built stainless steel chamber equipped with thin (0.04 mm) Kapton windows that transmit x-rays with virtually no attenuation or scattering at this energy. A diagram of the levitation instrument is shown in figure 2. The instrument was integrated with beamline 11 ID-C at the Advanced Photon Source (APS), USA. The experiment was performed in transmission geometry and diffraction patterns were collected using a Mar345 image plate detector carefully mounted orthogonal to and centered about the x-ray beam. The direct beam was blocked with a short length of 3 mm diameter tungsten rod that was mounted in front of the image plate. An image plate area detector was employed instead of an energy-discriminating point detector because the structure changes in CA melts and supercooled liquids are highly metastable (occasionally minute single crystals were observed to suddenly form when the droplet orbit became unstable and touched the levitation nozzle, only to re-melt in the undercooled liquid). Therefore a fast (area) detector system was suitable. The advantages of fast measurements are also important in the study of transient structural changes which may be observed on supercooling, as has been recently demonstrated by Hennet *et al* [10].

Samples of 2–3 mm in diameter were made from binary $(CaO)x\cdot(Al_2O_3)(1-x)$ compositions containing $x = 50$, 57, 62.5, 63, 64 and 67 mol% CaO. Negligible mass loss (<1%) was detected and after the high temperature levitation runs indicating that there are no significant changes in composition during the experiment. The samples were levitated in a flow of pure argon gas and melted with the laser beam from above. An x-ray beam of 1 mm × 1 mm in size was directed only onto the top half of the sample, above the equator corresponding to the top of the levitation nozzle. The image plate was exposed for eight, 30 s intervals. The use of short data acquisition runs prevented saturation of the detector if crystallization occurred. Data from eight runs was summed to improve the counting statistics. The image plate was erased after each exposure and for several times if saturation occurred, until the Bragg peaks disappeared. No Bragg peaks from the levitation nozzle were observed in any liquid spectra.

3. Data reduction

The sample–detector distance (449.4 mm) and tilt angle (0.722°) of the image plate were found by the refinement of a polycrystalline CeO_2 standard, using the software *FIT2D* [11]. A software mask was applied to the lower portion of the two-dimensional image plate data to discard scattering from the sample which had been attenuated by the levitation nozzle.

For a liquid where density fluctuations are governed by the diffusive part of the isothermal compressibility, the corrected

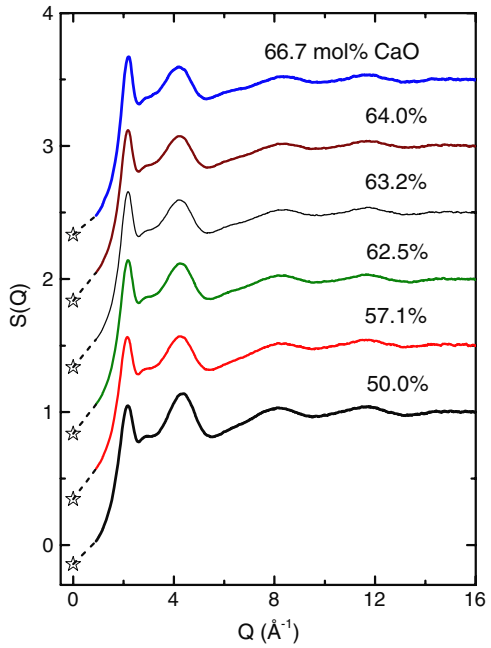

Figure 3. The measured high energy x-ray structure factor $S_X(Q)$ for the CA liquids for several compositions. Also shown are the calculated $S(0)$ limits (stars; see equations (1)) and dashed lines interpolating to the first measured point in the $S(Q)$ spectra. Curves are offset for clarity.

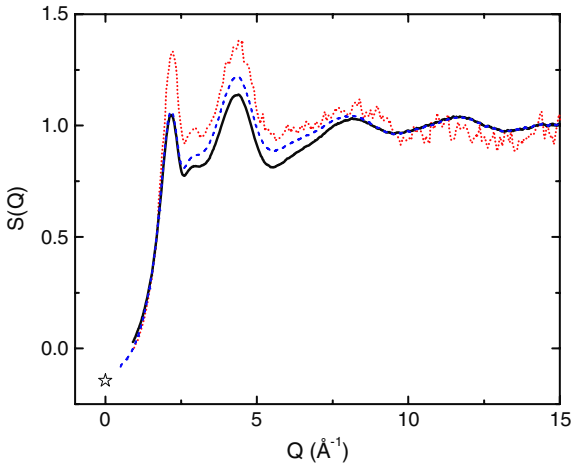

Figure 4. Comparison of the total x-ray structure factor for the 50%CaO:50%Al_2O_3 liquid from this study (thick black line represents measured $S(Q)$; blue dashed line represents $S(Q)$ after removal of the unphysical oscillations at low r) and previously published data (red dotted line) [16]. Also shown are the calculated $S(0)$ limits (stars, see equation (1)).

x-ray intensity may be written as [12]

$$S(Q=0)-1 = \left(\rho K_B T \chi_T(T) - \sum_i c_i f_i^2(0)\right) \Big/ \left(\sum_i c_i f_i(0)\right)^2 \quad (1)$$

where ρ represents the number density, $\chi_T(T)$ is the isothermal compressibility of the liquid at temperature T and $f_i(Q)$ represents the form factors. For these experiments we assume that $\rho K_B T \chi_T(T) \sim 0$ and there is negligible charge transfer between ions, reducing equation (1) to $S(Q=0)-1 = (-\sum_i c_i Z_i^2)/(\sum_i c_i Z_i)^2$. This limit is represented by the stars in figures 3 and 4.

The x-ray structure factors, $S_X(Q)$, shown in figure 3 were obtained up to $Q \sim 16$ Å^{-1} using the program *PDFGETX2* [13] by applying standard corrections as well as those required for the image plate geometry, including a constant subtracted from the background at the level of 10%. This offset value was iteratively determined by comparing the structure factor to the calculated $S(0)$ value described above. The additional correction is not due to sample attenuation which has typical values around 0.98–0.99 across our compositional range. A separate background measurement performed a few mm above a levitated crystalline sapphire sphere was also made as a function of temperature to investigate the effect of the density of the levitation gas on the background at different temperatures. Only effects at the 1.5% level were found between 1900 °C and room temperature. A likely explanation for this relatively small residual offset is the difficulty in completely erasing the phosphor screen of the image plate detector, an inherent problem with these types of detectors despite their low background. Nonetheless, the relatively small differences between the reduced $S(Q)$ and the Fourier back-transform (where the unphysical low-r oscillations have been removed) are shown in figure 4 and indicate the reduced $S(Q)$'s are reasonable.

The apparent temperature of the levitated sample was measured using an optical pyrometer (Mikron model M90-V, Mikron Infrared, Inc., Oakland, NJ) that operated at a wavelength of 0.650 μm. The pyrometer was equipped with two lenses that enabled imaging of the small droplets at a working distance of approximately 0.2 m. The pyrometer viewed the sample through a clean optical quality Pyrex window installed in the chamber. Apparent temperatures acquired from the pyrometer output were corrected to give the true temperature using Wien's approximation to Planck's law and the corrected temperatures are reported throughout this paper. Temperature corrections were made for reflections from the surfaces of the two lenses, surfaces of the Pyrex window and the emissivity of the sample. The latter was calculated to be 0.92 from the estimated index of refraction of the liquid. Thus, the effective emissivity used to correct the apparent temperatures was 0.716, obtained by accounting for the three factors described above. The estimated temperature measurement errors due to emissivity errors and temperature gradients that occur in the melt are ±25 °C. Measurements are shown at ∼1810 °C for all the CA liquids, as shown in figure 1. Details of the temperature measurement correction procedures have been reported elsewhere [14].

4. Results

The measured x-ray structure factors and radial distribution functions obtained using the densities given in [15] for CA liquids and our previous paper on glasses [1] are shown in figures 3–8. Hennet *et al* [16] have measured the x-ray

structure factor of liquid 50%CaO:50%Al_2O_3 and we compare this digitized curve to our data in figure 4. The main difference between the curves is the presence of a downward slope towards high Q on the data in [16], causing a shift in the position of the first peak. The temperature dependence of $S(Q)$ for the 64% CaO (eutectic) liquid shows little variation between 1970 and 1600 °C, yet the spectra are still significantly different from the room temperature glass. This supports the work of Hennet *et al* [16] who have argued that large structural variations do not occur in this liquid until much lower temperatures close to $1.25T_g = 1031$ °C for the eutectic composition [17].

Figure 5 shows the radial distribution function $G(r)$ for the CA liquids and figure 6 compares the liquid and glassy structure factors. Figure 7 reports the differential distribution function $D(r)$ for the 66.7% and 57.1% CaO liquids, in comparison with their glassy analogs. From the first peak position in the radial distribution function we find the Al–O bond distance in the liquid elongates slightly from 1.79±0.1 Å in CA glasses to 1.81±0.1 Å, and the Ca–O correlation appears as a weak feature around 2.3 Å. On the basis of bond valence theory [18] this is consistent with the dominant Al species being coordinated by four oxygens in both the liquid and the glass and may simply reflect the thermal expansion of the AlO_4 tetrahedra at higher temperatures. We also note that, in the CA2 (33.3% CaO) crystal [19], the Al–O bond distance is 1.806 Å for a tetrahedral tricluster and 1.715 Å (67%) and 1.778 Å (33%) for non-tricluster tetrahedra. Similarly the CA6 (14.3% CaO) crystal, which consists of AlO_6, AlO_5 and AlO_4 units [20] has a Al–O bond distance in the range of 1.806–1.999 Å for AlO_5 and AlO_6 polyhedra; and the Al–O bond distance varies in the range of 1.795–1.810 Å for AlO_4 polyhedra. This suggests that typically a 2–5% increase in the Al–O bond length may be associated with the formation of AlO_4 tetrahedral triclusters from a non-tricluster AlO_4 network, and on average there is a 6% increase in the Al–O bond length associated with the formation of higher coordinate polyhedra in the CA system. Since no significant change is measured in the Al–O bond length in the liquid compared to the glass in this study (∼1%, around the limit of the error), we interpret this as an indication that the melt is dominated by AlO_4 tetrahedra, although the formation of a significant fraction of tetrahedral triclusters and AlO_5, AlO_6 units in the melt is certainly possible.

Hennet *et al* [16] fitted Gaussians to the Al–O and Ca–O peaks in the x-ray diffraction data to give coordination numbers of 4.5 ± 0.5 and 5.5 ± 0.5 for the CA liquid at 1900 °C. They also found similar values of 4.4 ± 0.5 for the Al–O peak and 5.4 ± 0.5 for the Ca–O for Al–O and Ca–O from neutron measurements on the liquid using the same analysis [21]. An estimate of our Al–O coordination number using just the first half of the peak in $G(r)$, and assuming it is symmetric, gives a value of 4.2 ± 0.5, but with a similarly large error bar.

The position of the high-r shoulder on the first peak around 2.3 Å is most clearly observed in the 66.7% CaO composition (shown in the top plot in figure 5). Weighted differences taken between radial distribution functions at different concentrations and the 50% CaO function have been

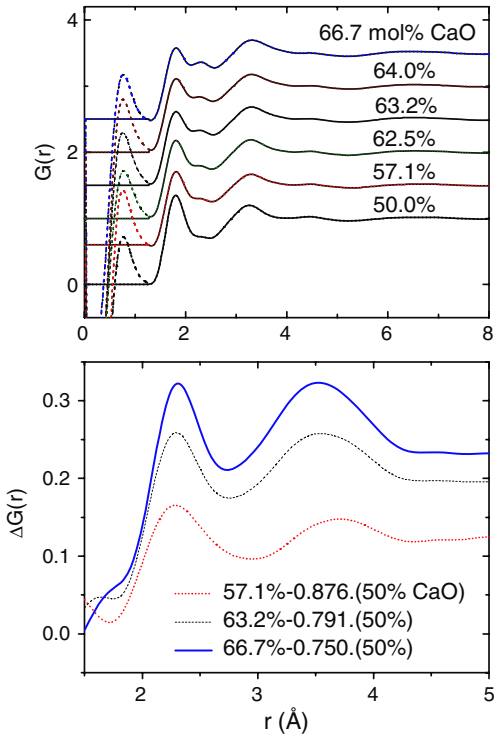

Figure 5. Top: the radial distribution functions $G(r)$ for the CA liquids (solid line) obtained from a Fourier transform of the curves shown in figure 3, with the unphysical oscillations shown as dotted lines at low r. The data were truncated at $Q_{max} = 16$ Å^{-1} and Fourier-transformed with a Lorch modification function [29]. The curves are offset for clarity. Bottom: the differences $\Delta G(r) = G^X(r) - (50/x)G^{50}(r)$ obtained for $x = 57.1\%$, 63.2% and 66.7% highlight the increase in Ca–O correlations.

obtained using the formula $\Delta G(r) = G^X(r) - (50/x)G^{50}(r)$, where x represents the mole fraction of CaO. These are shown in the bottom plot of figure 5 for $x = 57.1\%$, 63.2% and 66.7%. In the difference curves, the position of the CaO peak is clearly resolved and is found at a distance of 2.28 ± 0.03 Å for $x = 57.1\%$, 2.29 ± 0.02 Å for $x = 63.2\%$ and is at 2.31 ± 0.02 Å for $x = 66.7\%$. These Ca–O distances are consistent with a Ca–O coordination of about five on the basis of bond valence theory, which predicts a Ca–O distance of 2.22 Å for fourfold coordinated Ca by oxygen, 2.31 Å for fivefold and 2.37 for sixfold [22]. We note that crystal structures in this region (CA, C2A) typically have Ca ions sevenfold coordinated by oxygen with Ca–O bond distances ranging from 2.31 to 2.82 Å. These peak distances are similar to those obtained by Hennet *et al* [16, 21] who found a peak at 2.34 ± 0.03 Å using neutron data and 2.30 ± 0.05 Å using x-ray data for the 50% CaO composition. However, additional CaO correlations at longer distances may be likely based on the glass results discussed in our preceding paper. The Ca–O coordination numbers were not calculated directly in this study due to the heavy overlap of the Al–O and Ca–O peaks in the liquids and the complication of the observed shift in Ca–O peak position between the liquid at 1810 °C and the glass.

The third peak and high-r shoulder in the glassy x-ray radial distribution functions (see figure 7) are expected to have

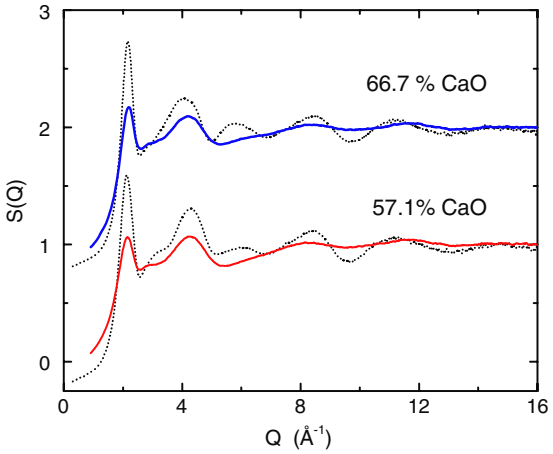

Figure 6. The measured high energy x-ray structure factor $S_X(Q)$ for the 66.7% CaO (thick blue line) and 57.1% CaO liquids (red line) in comparison with those for the corresponding CA glasses (black dotted lines). Curves are offset for clarity.

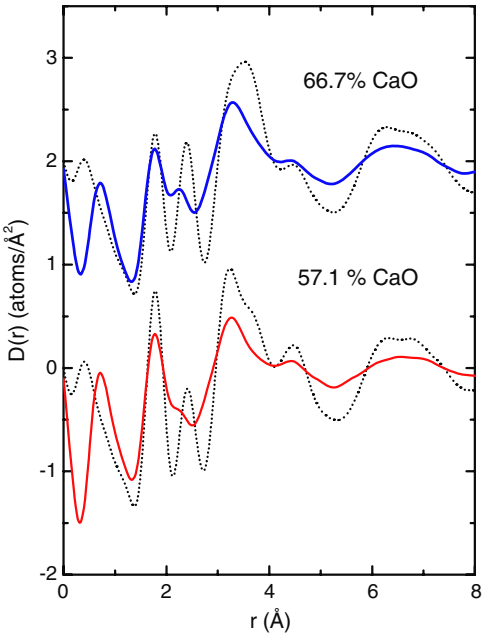

Figure 7. The radial distribution functions $D_X(r)$ for the 66.7% CaO (thick blue line) and 57.1% CaO (red line) liquids, obtained from a Fourier transform of the curves shown in figure 6, in comparison with those of CA glasses (black dotted lines). The data were truncated at $Q_{max} = 16$ Å^{-1} and Fourier-transformed with a Lorch modification function [29]. The curves are offset for clarity.

contributions from the Al–Al (∼3.1 Å), Ca–Al (∼3.4 Å), Ca–Ca (∼3.5 Å) and O–O (∼3.3 Å) correlations on the basis of recent molecular dynamics simulations [23, 24]. Also of importance for our work is the second-nearest neighbor Al–O_{II} distance, which is expected to be at ∼4.43 Å.

5. Discussion

The main changes observed in the liquid spectra compared to the glass are manifested by a large reduction in the height of the first diffraction peak in $S(Q)$ (see figure 6) and a broadening of the oscillations between $Q = 7$ and 13 Å^{-1}. The first peak at 2.20 Å^{-1} in 66.7% CaO liquid shifts to 2.17 Å^{-1} in the 50% CaO liquid, with a reduction in intensity as the Al_2O_3 fraction increases. The intensities of the features at 2.93 and 5.90 Å^{-1} also decrease with increasing Al_2O_3 fraction. The high Q oscillations beyond 7.0 Å^{-1} are associated with short range order structure and remain similar for all CA liquids, and these features are much more diffuse than those of the corresponding glasses.

Previously, Poe *et al* [2] have suggested, based on ion dynamics simulations, that the proportion of AlO_5 and AlO_6 might increase with increasing temperature in CA liquids: however, there is no significant change in our results for the eutectic liquid measured over a 370 °C temperature range, so any changes in population in this temperature region are likely to be minor. In more recent molecular dynamics simulations Wu *et al* [24] suggest that the Al–O coordination is tetrahedral across the entire compositional range of the melt. This is consistent with our interpretation, based on the relatively small increase in Al–O bond length between the liquid and the glass described previously. Wu *et al* [24] also predict an increase in tetrahedral tricluster population with increasing Al_2O_3 content, which is associated with a broad increase in the Al–Al partial around 4.5 Å. Our sensitivity to this partial structure is low in this experiment but a consequence of this structural change

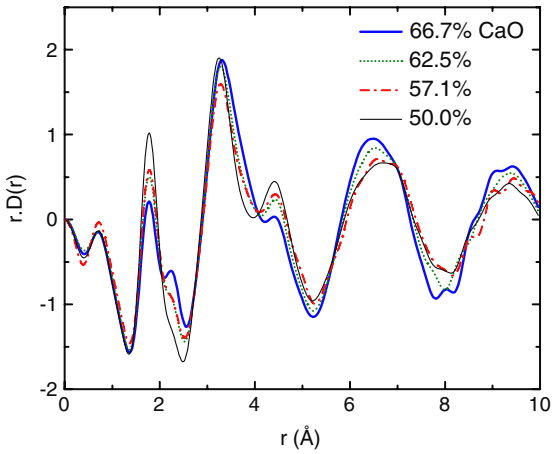

Figure 8. The radial distribution functions $r\,D_X(r)$ for the CA liquids obtained from a Fourier transform of the curves shown in figure 3. The data were truncated at $Q_{max} = 16$ Å^{-1} and Fourier-transformed with a Lorch modification function [29].

may appear indirectly in other correlations, particularly the Al–O and Ca–O.

Figure 7 shows the distribution functions $D(r) = 4\pi\rho r[G(r) - 1]$ for the 66.7% and 57.1% CaO liquids, in comparison with glasses. The most dramatic change in the liquid $D(r)$ compared to the glass is the broadening and shift of the Ca–O correlations, suggesting that Ca polyhedra are highly distorted in the liquid state. In both the 66.7% and 57.1% CaO distribution functions the CaO peak shifts from ∼2.40 Å in the glass to ∼2.25 Å in the liquid. The third peak in the

x-ray radial distribution function (figure 7) also changes, from a broad feature at ∼3.3 Å in the liquid state to a peak at ∼3.5 Å in the 66.7% CaO glass and a peak at 3.23 Å plus a shoulder at ∼3.6 Å in glassy 57.1% CaO. At composition 66.7% CaO, the increase in intensity of the third peak in the glass compared to the liquid appears to be entirely due to the sharpening of the local Ca–O peak, i.e. the existence of more well-defined CaO_n polyhedra and enhanced connectivity, as no significant changes occur in the intensity of the Al–O_I (1.81 Å) or AlO_{II} (4.46 Å) peaks. This is not the case at 57.1% CaO where both sharper Al–O and CaO peaks appear in the glass radial distribution function. A possible explanation for this is that at 67 mol% CaO the Al framework is already broken up and only exists in small fragments, whereas at 57 mol% CaO the Al network is still the dominant network. A similar situation has been found close to the Mg_2SiO_4 composition around 67 mol% MgO [26] where the dominant network component changes from SiO_4 to MgO_n ($n = 4, 5, 6$) when the silica content is decreased.

The barely resolved CaO peak in the 50% CaO liquid shown in figure 5 has also been reported by Hennet *et al* [16]. However, these authors also report a series of short experiments on supercooled and glassy 50% CaO which show no distinct CaO peak which may be an artifact of their limited Q range. A consequence of the observed shift in CaO peak position between the CA liquids and glasses (in figure 7) is that it will influence the first peak position and change in Al–O coordination number as a function of temperature as T_g is approached. This confirms the concern of Hennet *et al* (equation (2) in [16]) that their first peak position values are affected by changes in the overlapping CaO peak. Interestingly, these authors [16] report a kink in the cooling curve of a 50%CaO:50%Al_2O_3 liquid in an aerodynamic levitator and attribute this feature to a change in the melt's thermodynamic properties. If so, this would provide a valuable connection between the thermodynamic and kinetic fragility of the melt. However, we suggest an alternative explanation, by noting that the dominant heat transfer mechanism shifts from radiation (T^4) to convection (T linear) at ∼1200 °C (where T = temperature) and there is an associated change in slope of T versus time when this occurs. There can also be changes in emissivity at lower T where some oxide melts become partially transparent.

The structural variations with composition in the liquid state at higher distances are highlighted in figure 8 by showing the function $rD(r)$. This plot tentatively indicates that compositional changes may not have a linear effect on structure. Between 57.1% and 62.5% the local Al–O and Ca–O polyhedral structures are very similar, with the main structural changes occurring around the 6.63 Å peak which is tentatively attributed to Ca-related correlations. On the basis of molecular dynamics simulations Wu *et al* [25] have argued that the existence of triclusters through bridging oxygens is responsible for charge balance in the melt and the location of the Ca ions. In their simulations the CaO coordination number decreases slightly with increasing CaO content from 6.1 at 50 mol% CaO to 5.5 at 70 mol% CaO. However, no details of the simulation CaO radial distribution function is reported to compare to our data.

In terms of our diffraction measurements one possible explanation based on the crystal structures is a change in the Ca–Ca edge:face sharing ratio. This model, although speculative, may be used to explain the shift of the local Ca–O (probably through a redistribution of correlations to higher r values) in the glass compared to the liquid at the eutectic composition. We note that for Mayenite (C12A7, 63.2% CaO), the edge sharing Ca–Ca distance is 3.679 Å, and for C5A3 (62.5% CaO), edge sharing distances can be as short as 3.21 Å, whereas the corner sharing Ca–Ca distances are as long as 4.90 Å. However, the cause of the redistribution of Ca–O bonds is likely to be a consequence of changes in the strong Al–O framework. The data are therefore consistent with the OAl_3 tricluster model previously proposed by McMillan and coworkers [4]. If so, this would tend to suggest that the structural changes are driven by a competition for oxygen and reflect the ability of more structural configurations to be accessed in the liquid state compared to the glass. Moreover, the variation in Ca–O coordination number between different glass studies suggests that the glass structure may well be sensitive to quench rate. Compositional and connectivity changes between polyhedra near the eutectic composition are most likely associated with the opposite trends observed for the O–O peaks in the 3–4 Å region of $G_X(r)$ between the 57 mol% and 67 mol% CaO compositions in the glassy and molten states.

Given the differences in CaO peak distances between the glass and liquid states in the CA system, the important role of oxygen may be an important factor in determining how the liquid structure evolves with temperature. At high temperatures, increased entropy may tend to evaporate oxygen from the melt. If the liquid is then rapidly cooled, it may result in a small oxygen deficit and hence modify the resulting structure [26].

6. Conclusions

In CA melts, the almost identical position of the first peak in the radial distribution function, compared to the glass suggests that AlO_4 species remain the dominant aluminate polyhedra. It is also found that the structure for the eutectic (64% CaO) liquid does not change measurably with temperature between 1600 and 1970 °C. However, a dramatic broadening of the Ca–O peak occurs in the liquid spectra compared to the glass and the shift in position of the shoulder to 2.25 Å indicates that, on average, each Ca is surrounded by five oxygen atoms in the melt on the basis on bond valence theory, although additional Ca–O correlations at longer distances are possible. The Ca disorder appears to be the main structural change between the liquid and the glass at the 66.7% CaO composition, whereas both Ca and Al disorder occur in the liquid at the 57.1% CaO composition. This may indicate the number of Al units have become dilute enough by 67 mol% CaO that the Al network has become largely de-polymerized. For future work more detailed molecular dynamics simulations are required to fully explain the observed differences in CaO correlations between the liquid and glassy states in these fragile materials.

Acknowledgments

Professor Paul McMillan is thanked for useful discussions regarding [5]. This work was supported by the US DOE, at the XSD and IPNS Divisions, Argonne National Laboratory under contract no. DE-AC02-06CH11357 and partially supported by NASA contract no. NMM04AA23G.

Note added in proof. It has come to our attention that a new NMR heteronuclear correlation technique has recently provided comprehensive experimental proof of the presence of ∼5% oxygen triclusters in $CaAl_2O_4$ glass [30] representative of the liquid state structure at $T_g = 1180\,^{\circ}C$.

References

[1] Mei Q, Benmore C J, Siewenie J, Weber J K R and Wilding M 2008 *J. Phys.: Condens. Matter* **20** 245106
[2] Poe B T, McMillan P F, Cote B, Massiot D and Coutures J-P 1994 *J. Am. Ceram. Soc.* **77** 1823
[3] Poe B T, McMillan P F, Cote B, Massiot D and Coutures J-P 1993 *Science* **259** 786–8
[4] Daniel I, McMillan P F, Gillet P and Poe B T 1996 *Chem. Geol.* **128** 5–15
[5] McMillan P F, Petuskey W T, Cote B, Massiot D, Landron C and Coutures J P 1996 *J. Non-Cryst. Solids* **195** 261–71
[6] Urbain G 1983 *Rev. Int. Hautes Temp. Refract.* **20** 135
[7] Krishnan S, Felten J J, Rix J E, Weber J K R, Nordine P C, Beno M A, Ansell S and Price D L 1997 *Rev. Sci. Instrum.* **68** 3512–8
[8] Mei Q, Benmore C J and Weber J K R 2007 *Phys. Rev. Lett.* **98** 057802
[9] Poulsen H F, Neuefeind J, Neumann H B, Schneider J R and Zeidler M D 1995 *J. Non-Cryst. Solids* **188** 63
[10] Hennet L, Krishnan S, Bytchkov A, Key T, Thiaudiere D, Melin P, Pozdnyakova I, Saboungi M L and Price D 2005 *Int. J. Thermophys.* **26** 1127–36
[11] Hammersley A P 1998 *FIT2D Internal Report ESRF98HA01T* European Synchrotron Radiation Facility, Grenoble, France
[12] Egelstaff P A 1992 *Introduction to the Liquid State* 2nd edn (Oxford: Clarendon) p 30
[13] Qiu X, Thompson J W and Billinge S J L 2004 *J. Appl. Crystallogr.* **37** 678
[14] Weber J K R, Krishnan S, Anderson C D and Nordine P C 1995 *J. Am. Ceram. Soc.* **78** 583–7
[15] Paradis P F, Yu J D, Ishikawa T and Yoda S 2003 *J. Am. Ceram. Soc.* **86** 2234–6
[16] Hennet L, Pozdnyakova I, Bytchkov A, Price D L, Greaves G N, Wilding M, Fearn S, Martin C M, Thiaudière D, Bérar J-F, Boudet N and Saboungi M-L 2007 *J. Chem. Phys.* **126** 074906
[17] Uhlmann E V, Weinberg M C, Kreidl N J and Gokta A A 1993 *J. Am. Ceram. Soc.* **76** 449
[18] Shannon R D and Prewitt C T 1959 *Acta Crystallogr.* B **25** 925
[19] Ponomarev V I, Kheiker D M and Belov N V 1970 *Kristallografiya* **15** 1140–3
[20] Utsunomiya A, Tanaka K, Morikawa H, Marumo F and Kojima H 1988 *J. Solid State Chem.* **75** 197–200
[21] Hennet L, Pozdnyakova I, Cristiglio V, Krishnan S, Bytchkov A, Albergamo F, Cuello G J, Brun J-F, Fischer H E, Zanghi D, Brassamin S, Saboungi M-L and Price D L 2007 *J. Non-Cryst. Solids* **353** 1705
[22] Hannon A C and Parker J M 2000 *J. Non-Cryst. Solids* **274** 102
[23] Kang E T, Lee S J and Hannon A C 2006 *J. Non-Cryst. Solids* **352** 725–36
[24] Thomas B W M, Mead R N and Mountjoy G 2006 *J. Phys.: Condens. Matter* **18** 4697–708
[25] Wu Y, You J and Jiang G 2003 *J. Inorg. Mater.* **18** 619–26
[26] Kohara S, Suzuya K, Takeuchi K, Loong C K, Grimsditch M, Weber J K R, Tangeman J A and Key T S 2004 *Science* **303** 1649–52
[27] Chatterjee A K and Zhmoidin G I 1972 *J. Mater. Sci.* **7** 93
[28] Nurse R W, Welch J H and Majumdar A J 1963 *Trans. Br. Ceram. Soc.* **64** 416
[29] Lorch E A 1969 *J. Phys. C: Solid State Phys.* **2** 229
[30] Iuga D, Morais C, Gan Z, Neuville D R, Cormier L and Massiot D 2005 *J. Am. Chem. Soc.* **127** 11540